LETTER

Universality of steric effects of electrolytes in nanoconfinements

A Letters Journal Exploring the Frontiers of Physics

October 2018

EPL, **124** (2018) 14004 www.epljournal.org
doi: 10.1209/0295-5075/124/14004

Universality of steric effects of electrolytes in nanoconfinements

Rajni[1], I. S. Kang[2] and J. M. Oh[2,3]

[1] *Jindal Global Business School, O.P. Jindal Global University (JGU) - Sonipat, Haryana-131001, India*
[2] *Department of Chemical Engineering, Pohang University of Science and Technology (POSTECH) Pohang 37673, Republic of Korea*
[3] *Center for Soft and Living Matter, Institute for Basic Science (IBS) - Ulsan 44919, Republic of Korea*

received 7 August 2018; accepted in final form 8 October 2018
published online 9 November 2018

PACS 47.57.jd – Electrokinetic effects
PACS 61.20.Qg – Structure of associated liquids: electrolytes, molten salts, etc.
PACS 41.20.Cv – Electrostatics; Poisson and Laplace equations, boundary-value problems

Abstract – We analyze the steric effect of electrolyte on the normal stress exerted on a wall and the free charge density in a nanoconfinement using the modified Poisson-Boltzmann (mPB) equation. The outward normal stress exerted on the channel wall (P_{nn}) is calculated by solving the mPB numerically with a constant surface potential for various equilateral polygonal channels and compared with one-dimensional and circular channels by varying the steric factor (γ) and asymmetry of ions (ξ). The results show that the averaged normal stress on the walls ($\overline{P_{nn}}$) and the averaged charge density in the channels ($\overline{\rho}$) are almost independent of the channel shape, and are the same with those of the circular channel. From the numerical observation, we infer the universality of average electric field ($\overline{E_n}$) and average electrical stress ($\overline{E_n^2}$) on the channel wall, both of which are independent of the channel shape if the hydraulic radius is the same.

Introduction. – The phenomenon of electrolyte in a nanoconfinement has been studied for a long time before we began to understand our interest in nanoparticles or nanostructures in the name of nanoscience. It is found in many examples such as reactions of catalysis coated on porous structures, charging/discharging phenomena in porous electrodes in batteries, and desalination of seawater based on selective ion exchange membranes [1–7]. In these applications, an important question is how much ion can be charged to the porous structure, or how much force the porous structure receives from the electrolyte, and whether the structure is indeed sustainable by the force. This is because the force exerted on the wall and the charge density in the nanostructure caused by the electrolyte are the primary factors that can affect the efficiency and durability of the system directly.

In terms of the efficiency and durability of applications, research has been limited except for experimental verification. However, in experiments, it is difficult to understand the structural characteristics of an electric double layer (EDL) systematically because it is difficult to directly observe the ion distribution in a nanostructure. Particularly, because the theoretical understanding is primarily limited to a one-dimensional (1D) slit, researches on the characteristics of the EDL structure in various situations are scarce.

In general, the force exerted on a channel wall and the charge density in a porous structure can be predicted by solving the electric field and distribution of ions in the domain. In many cases, the conventional Gouy-Chapman theory or the Poisson-Boltzmann (PB) equation derived from the theory is sufficient. However, when the EDL thickness and channel size become comparable and the ion concentration is increased significantly owing to the high potential, the ion-ion interaction and the finiteness of ion size become paramount. Consequently, the real EDL structure can be quite different from the PB model. An electrolyte in a charged slit can induce an overcharging and charge reversal owing to the effects of unequal ionic sizes with respect to the concentration, ion size and valence [8]. The effective extent of the EDL overlap can also be caused by the nontrivial interaction between the steric effect and EDL overlap in narrow fluidic confinement [9]. This can be explained by the modified PB (mPB) based on the mean-field theory developed by several researchers. Further, many researchers have recently reported their progresses on the steric effect and the correlation effect using this model [10–12].

In many application problems, a nanoconfinement is not simply a 1D slit or circular channel, but exhibits a complex network structure with various shapes of its cross-section. Theoretical studies on the steric effect of various channel

shapes do not exist even though many have been published for the 1D slit or circular channel with or without steric effects [10,11,13–17]. To realize various channel shapes, we consider a channel with equilateral polygonal shape as the cross-section, and nine types of channels from triangle to 72-polygon are analyzed. The results will be compared with the results of the 1D slit and circular channel.

Herein, we first review the characteristics of the mPB model with respect to the steric factor, and subsequently analyze the EDL structure (*i.e.*, osmotic pressure, ion concentration, electric force distribution, etc.) in various channel shapes. We found that the averaged normal stress exerted on the wall and the averaged charge density in the channel remain almost constant regardless of the channel shape if the hydraulic radius is the same. Hence, we will discuss the universality of electric field and electrical stress on the channel wall.

Modified Poisson-Boltzmann equation and osmotic pressure. – The effect of finite ion sizes can be characterized via the compressibility as $\gamma = 2a_+^3 c_0$, where a_+ is the size of the cation, and c_0 is the initial bulk number density [3,18]. Therefore, γ is also known as the volume fraction of ions for the same-sized ions [10]. When γ approaches 1, the salt-only electrolytes are completely packed without vacancy. To consider the size difference of the cation and anion, the anion/cation volume ratio (asymmetry factor) is introduced as $\xi = V_-/V_+ = a_-^3/a_+^3$, where a_- is the size of the anion [15,18]. We assume that the anion is smaller than the cation ($0 < \xi \leq 1$). From the equilibrium condition together with the chemical potential in the mean-field theory, one can derive the dimensionless number density of the cation (c_1) and anion (c_2) [18],

$$c_1 \equiv \frac{c_+}{c_0} = \frac{N_+}{N_0} = \frac{2}{\gamma}\frac{\exp(-u)}{\exp(-u) + (\xi+\eta)\left[\frac{\xi\exp(u)+\eta}{\xi+\eta}\right]^{\frac{1}{\xi}}}, \quad (1)$$

$$c_2 \equiv \frac{c_-}{c_0} = \frac{N_-}{N_0} = \frac{2}{\gamma}\frac{\exp(u)\left[\frac{\xi\exp(u)+\eta}{\xi+\eta}\right]^{\frac{1}{\xi}-1}}{\exp(-u) + (\xi+\eta)\left[\frac{\xi\exp(u)+\eta}{\xi+\eta}\right]^{\frac{1}{\xi}}}, \quad (2)$$

where the porosity in the bulk is defined by $\eta = 2/\gamma - 1 - \xi$ and the dimensionless potential (u) is expressed by

$$u = \frac{e\psi}{k_B T} = \frac{\psi}{V_{th}}.$$

Here, e is the electron charge, k_B is the Boltzmann constant and T is the absolute temperature of the system. The thermal voltage (V_{th}) is approximately 25.85 mV for $T = 300$ K. The dimensionless ion concentrations, c_1 and c_2, are dependent on only the electrical potential and the size of ions (γ and ξ). Equations (1) and (2) are reduced to the Gouy-Chapman theory for $\gamma \to 0$. Figure 1(a) represents the potential dependence on c_1 and c_2 for $\gamma = 0.2$, 0.5 and 1.0 at $\xi = 0.5$. The saturated concentrations are given as $2/\gamma$ and $2/\gamma\xi$ for c_1 and c_2, respectively [18].

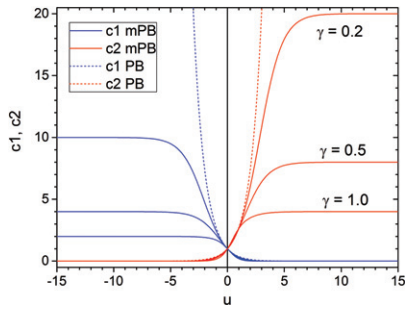

(a)

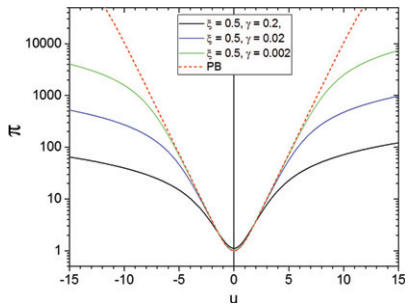

(b)

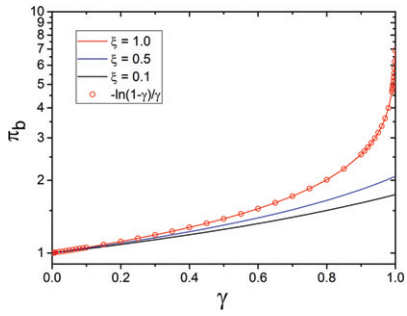

(c)

Fig. 1: (Color online) Potential dependence of (a) the ion concentrations at $\gamma = 0.2$, 0.5 and 1.0 and $\xi = 0.5$ and (b) the osmotic pressure at $\gamma = 0.002$, 0.02 and 0.2 with $\xi = 0.5$. (c) γ-dependence of π_b for $\xi = 0.1$, 0.5 and 1.

Further, the conventional Gouy-Chapman theory (dotted line in fig. 1(a)), which corresponds to $\gamma \to 0$, deviates significantly from the modified PB model even at low u.

The electric potential is governed by the Poisson equation and its dimensionless version is expressed by

$$-\epsilon^2 \nabla^2 u = \frac{1}{2}(c_1 - c_2) \quad (3)$$

with the Debye length ($\lambda_D = \sqrt{\varepsilon k_B T/2z^2e^2c_0}$) and the relative EDL thickness ($\epsilon = \lambda_D/H$). Here, H is the characteristic length scale of the system. Combining eqs. (1) and (2) with eq. (3) yields the mPB equation [15],

$$-\epsilon^2 \nabla^2 u = \frac{1}{\gamma}\frac{\exp(-u) - \exp(u)\left[\frac{\xi\exp(u)+\eta}{\xi+\eta}\right]^{\frac{1}{\xi}-1}}{\exp(-u) + (\xi+\eta)\left[\frac{\xi\exp(u)+\eta}{\xi+\eta}\right]^{\frac{1}{\xi}}}. \quad (4)$$

Equation (4) converges to the mPB equation for the symmetric electrolytes [10,18,19] at $\xi = 1$.

We can relate the osmotic pressure and the electric potential from the Navier-Stokes equations (NS) [15,20],

$$\boldsymbol{\nabla}\hat{\pi} = \rho_f \hat{\mathbf{E}}. \tag{5}$$

Using eqs. (4) and (5), the osmotic pressure can be derived as

$$\begin{aligned}\pi &= \frac{\hat{\pi}}{2c_0 k_B T} \\ &= \frac{1}{\gamma}\left[\ln\left(\exp(-u) + (\xi+\eta)\left[\frac{\xi\exp(u)+\eta}{\xi+\eta}\right]^{\frac{1}{\xi}}\right) + \ln\frac{\gamma}{2}\right] \\ &\quad + \pi_b,\end{aligned} \tag{6}$$

where π_b is the bulk pressure at $u = 0$. Here, the characteristic pressure π_c is set as $2c_0 k_B T$. The other method of deriving the osmotic pressure is to use the Helmholtz free energy, which is obtained from the mean-field theory [20]. The obtained osmotic pressure is expressed in the dimensionless form as

$$\begin{aligned}\pi = \frac{1}{\gamma}\Bigg[&\ln\left(\exp(-u) + (\xi+\eta)\left[\frac{\xi\exp(u)+\eta}{\xi+\eta}\right]^{\frac{1}{\xi}}\right) \\ &+ \left(\frac{1}{\xi}-1\right)\ln\left(\xi+\eta\right) - \frac{1}{\xi}\ln\eta\Bigg].\end{aligned} \tag{7}$$

Figure 1(b) shows the potential dependence on the osmotic pressure at $\xi = 0.5$ and $\gamma = 0.2, 0.02$ and 0.002. The dotted line represents the conventional PB equation, *i.e.*, for $\xi = 1$ and $\gamma \to 0$, which is represented by $\pi_{PB} = \cosh(u)$. The osmotic pressure increases exponentially with $|u|$ as $|u| \to \infty$. The osmotic pressure with steric effects deviates from the conventional PB prediction in a large extent even at a small γ at high $|u|(> 10)$. And, for $\gamma = 0.2$, the deviation starts even in low $|u|(< 5)$. A transition regime appears in slope, where π deviates from the conventional PB prediction. This transition regime implies that the ions are about to saturate.

The bulk pressure is obtained from eqs. (6) and (7),

$$\pi_b = \frac{1}{\gamma}\left[-\ln\frac{\gamma}{2} + \left(\frac{1}{\xi}-1\right)\ln\left(\xi+\eta\right) - \frac{1}{\xi}\ln\eta\right]. \tag{8}$$

As shown, π_b is monotonically increasing with respect to γ, and is similar to the Carnahan-Starling equation of state for a single species. Further, it converges to 1 as $\gamma \to 0$ (fig. 1(c)); this corresponds to the van 't Hoff law in low concentration limits ($\hat{\pi} = cRT$). The bulk pressure increases significantly as $\gamma \to 1$, where the ions are tightly packed without solvent. When the ions are symmetric ($\xi = 1.0$), eq. (8) converges to $-\frac{\ln(1-\gamma)}{\gamma}$ (hollow circles in fig. 1(c)) [15] and decreases with respect to ξ.

We now consider the normal stress exerted on the wall. The total stress tensor without the flow field is expressed as

$$\mathbf{T} = -\hat{\pi}\mathbf{I} + \mathbf{T}^e, \tag{9}$$

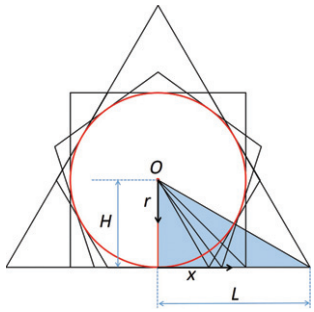

Fig. 2: (Color online) Schematics for cross-sections of polygonal channels and their domain definitions.

where $\mathbf{T}^e$ is the Maxwell stress. The normal stress exerted on the channel wall is

$$\hat{P}_{nn} = -T_{nn} = \hat{\pi} - \frac{\varepsilon\varepsilon_0}{2}\hat{E}_n^2. \tag{10}$$

$\hat{P}_{nn}$ is decreased by the electric field. The osmotic pressure is expressed only by the potential, thus implying that the osmotic pressure (π) is constant along the wall when the wall potential (V_0) is set on the wall. However, the electric field is varied and it induces a nonuniform normal stress distribution exerted on the wall.

EDL structure in various channels. – We are interested in the steric effect on $\hat{P}_{nn}$ for various nanoconfinements with a constant wall potential (V_0). Here, we consider nanochannels with various cross-sectional shapes that are equilateral polygons. The equilateral polygons are defined with the same hydraulic radius R_H, which is defined by $R_H = 2A/C$, where A is the cross-sectional area of the channel and C is its perimeter. The equilateral polygons circumscribe the circle of radius H as shown in fig. 2 [16].

The dimensionless stress normal to the E-field direction, which is scaled with $2c_0 k_B T$, is expressed as

$$P_{nn} = \pi - \frac{\epsilon^2}{2}E^2. \tag{11}$$

P_{nn} becomes the normal force exerted on the wall at the channel wall. P_{nn} is decreased by the electric stress and its upper bound is the osmotic pressure. It is noteworthy that P_{nn} is a function of u and $\boldsymbol{\nabla}u(= -\mathbf{E})$, not only u. Therefore, the normal stress distribution is not matched with the potential distribution. P_{nn} can be calculated numerically for various channels. The E-field is obtained by solving eq. (4) and π is calculated from eq. (7).

Figure 3 shows the results of the numerical analysis at $\xi = 1$, $\gamma = 0.2$, $\epsilon = 0.2$ and $V_0 = 10$ in various confinements as a color contour. Figure 3(a) shows the contour of E^2, which has the largest value on the wall, and decreases exponentially as it moves away from the wall. In a polygon, the electric field at the center of the edge is the highest, and the weaker field moves to the vertex, and converges to zero. This is because the electric field is vanishing at the vertex. Consequently, $\hat{P}_{nn}$ is highest at the

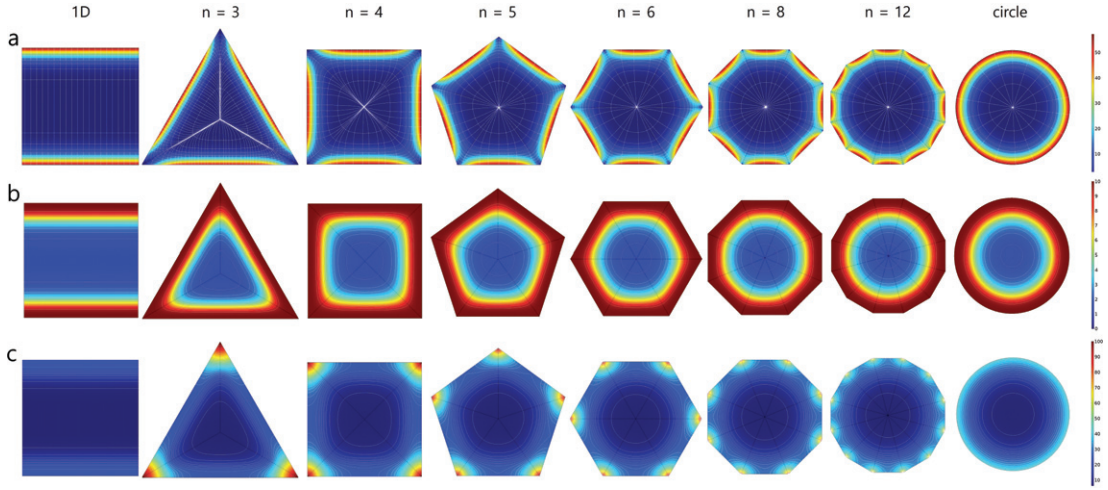

Fig. 3: (Color online) Numerically solved (a) E^2, (b) c_2 and (c) P_{nn} fields for the 1D channel, $n = 3$–12 and circular channel at $\epsilon = 0.2$, $\xi = 1$, $\gamma = 0.2$ and $V_0 = 10$.

vertex and decreases as n increases as shown in fig. 3(c). It is noteworthy that $\hat{P}_{nn}$ is the highest at the vertex rather than at the center of the edge. This implies that the corner portion of the nanochannels or porous media can be structurally vulnerable. $\hat{P}_{nn}$ at the vertex of the polygon converges to that of a circular channel as $n \to \infty$, as shown in fig. 4(d).

The electric potential u also decreases exponentially from the wall, but it is not completely screened, *i.e.*, $u \neq 0$ at $r = 0$. Figure 4(a) (u-profiles along $h = r/H$) shows that the potential is not zero at the center ($h = 0$). It is notable that the 1D channel case forms the lower bound of the profiles and the circular channel case forms the upper bound. This tendency is similar in the c_2-profile (fig. 3(b)). In the case of c_2, however, the potential u is 10 at the wall ($h = 1$) rather than decreasing exponentially from the wall. Therefore, the area of near saturation (c_2-profile is nearly flat as $u \to 10$) appears near the wall (see also fig. 1(a)). This saturation layer extends not only to the center of the edge but also to the vicinity of the vertex. As shown in fig. 3(b), the saturation layer (red region) is relatively thicker near the vertex owing to its geometric characteristics, unlike the E^2-distribution.

In the case of osmotic pressure (fig. 4(c)), there is no significant difference between the polygons and only a slight variation in the middle of the h-axis region. Because the osmotic pressure is a function of u only, all polygons fall off rapidly from the wall with the same value ($\pi \to 40$ at $u = 10$) on the wall (dropping to less than 1/10 already near $h = 0.7$ for $\epsilon = 0.2$). This is a large value because the osmotic pressure on the wall increases to 40 times the bulk pressure (assuming the actual concentration is 1 mM, it increases to $\mathcal{O}(200\,\mathrm{kPa})$). However, the actual normal stress exerted on the wall is much less than that, because the electric stress relieves the normal stress according to $P_{nn} = \pi - \frac{\epsilon^2}{2}E^2$. As shown in fig. 4(d), P_{nn} can be 10 times larger than the bulk pressure (π_b) at the wall (at a circular channel reference, $V_0 = 10$), which can also produce a relatively large pressure gradient. In particular, the normal stress (P_{nn}) in the h-axis direction, which is the sum of the osmotic pressure and electric stress, is constant along the h-direction for the 1D channel, *i.e.*, the pressure at the wall is equal to that in the center of the channel (black solid line in fig. 4(d)). The interpretation in the 1D channel is discussed in detail by Rajni *et al.* [15]. In the case of a triangle or a square, the normal stress (P_{nn}) exerted on the wall ($h = 1$) does not differ significantly from that in the 1D channel, and increases gradually as n increases, converging to the case of a circular channel. However, this tendency is limited to viewing in the h-direction from the center of the polygon edge. A significantly different change occurs along the wall, which will be discussed in the next section.

Normal stress exerted on channel wall. – Figure 5(a) shows the outward normal stress profile along the polygonal edge (L in fig. 2). The 1D channel has a constant value along the wall [15] and is the lower bound (black solid line). In the case of polygons, as shown in fig. 3, the normal stress is minimum at the center of the edges because the electric field is strongest at the center of the edges, and increases monotonically toward the vertex. P_{nn} at the vertex has an upper bound value, corresponding to the osmotic pressure at a given potential. The values of P_{nn} at the vertex for the triangle, quadrilateral, pentagon, and hexagon channels almost reach to the upper bound. For higher n, P_{nn} at the vertex is decreasing with the influence of the neighbor edges (dashed red line connected with hollowed circles) and converges to the P_{nn} in the circular channel wall (horizontal dashed black line). P_{nn} at the edge center converges to the P_{nn} of the circular channel as n increases, as shown in fig. 4(d), and is represented by black solid circles in fig. 5(a). As shown, P_{nn} exhibits a relatively large value change along the wall, and can be much larger than $P_{nn,\,circle}$ near the vertex. That is, the

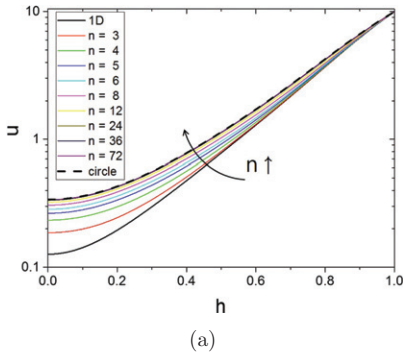

(a)

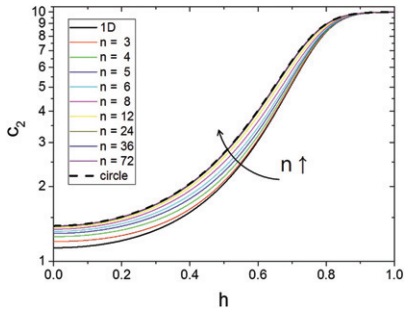

(b)

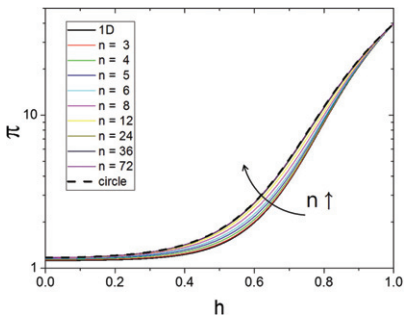

(c)

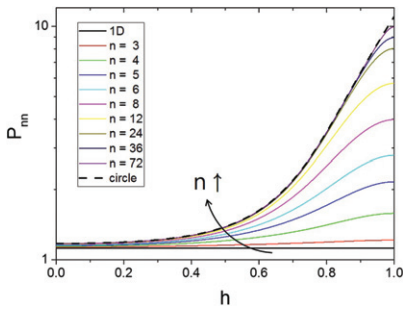

(d)

Fig. 4: (Color online) Profiles of (a) u, (b) c_2, (c) π and (d) P_{nn} in the h-direction of 1D, polygonal and circular channels at $\xi = 1.0, \epsilon = 0.2, V_0 = 10$ and $\gamma = 0.2$.

P_{nn} of the circular channel is not the upper bound, which is valid only along the h-axis as in fig. 4.

A more interesting part of this result is that the perimeter averages of P_{nn} of all polygons have almost the same values and are almost equal to the P_{nn} of circular channels. The average value of P_{nn} can be calculated by the

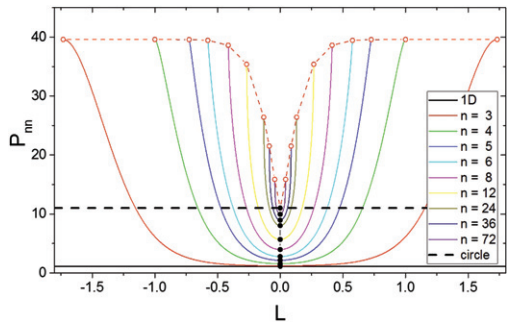

(a)

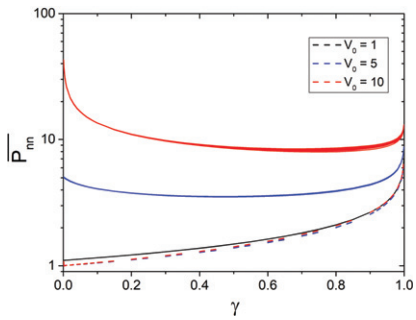

(b)

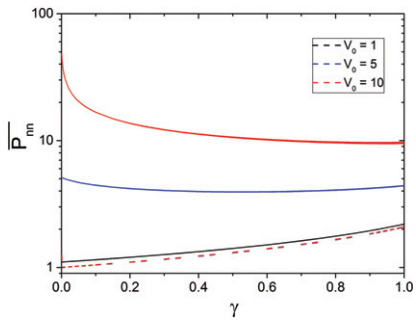

(c)

Fig. 5: (Color online) Normal stress exerted on the channel wall: (a) P_{nn} profile in the L-direction scaled with H, and γ-dependence on $\overline{P_{nn}}$ (b) at $\xi = 1.0$, (c) at $\xi = 0.5$ for $V_0 = 1, 5$ and 10 with $\epsilon = 0.2$. The dashed lines represent the corresponding 1D channel cases.

following equation:

$$\overline{P_{nn}} = \frac{1}{C} \oint_C P_{nn} \, \mathrm{d}l. \tag{12}$$

Figures 5(b) and (c) show the γ-dependence of the averaged normal stress $\overline{P_{nn}}$ for $\xi = 1.0$ and 0.5, respectively, which is the normal stress exerted on the wall, for all polygons, 1D and circular channels when $V_0 = 1, 5$, and 10. As shown in fig. 5, the same is observed as the γ and V_0 values change. The γ-dependence of the 1D channel is noteworthy. The $\overline{P_{nn}}$ profile with respect to γ is similar to that of the bulk pressure π_b, and almost no change occurs according to V_0 (three profiles almost overlap) (see also fig. 1(c)). This is because $\pi(h = 0)$ is the same as P_{nn} at the wall surface of the 1D channel, and it does not

change significantly according to V_0 at $\epsilon = 0.2$. In the case of the polygon at $V_0 = 1$, it is not significantly different from the 1D channel case because the electric field is not strong at the wall surface. As V_0 increases, the normal stress at the wall increases significantly because the ion concentration becomes high on the wall when γ is small. It is interesting to note that $\overline{P_{nn}}$ increases rapidly in the lower γ regime, but slowly in the higher γ regime so that the $\overline{P_{nn}}$-profile exhibits the minimum value in the middle of γ $(0 < \gamma < 1)$ at $V_0 = 5$ and 10 for $\xi = 1.0$. That is, the average value of the outward normal stress exerted on the channel wall is not minimized when the ions are perfectly packed, or when the ion size is negligibly small, but somewhere in between. This is not obvious for $\xi = 0.5$ because π_b does not increase significantly with respect to γ (see also fig. 1(c)). This tendency of the normal stress exerted on the channel wall can be an important physical characteristic when designing the size of the channel in applications using electrolytes. Most importantly, all of these tendencies are universal irrespective of the channel shapes except the 1D channel if R_H is the same.

Averaged free charge density in various channel shapes. – The local free charge near the wall is not neutral owing to the interaction between the ions and the charged wall [5], which is described by the mPB [10,15,18]. The role of the averaged free charge density becomes significant in nanoconfinement since the EDL occupies a large fraction over the channel such as nanoporous electrodes for energy storage applications. The nonzero averaged free charge density can be understood as ion enrichment in which the amount of one ion is larger than that of the other one. In this section, we calculate the averaged charge density ($\overline{\rho}$) over the cross-sectional area of the channels and analyze the geometrical effect and steric effect together with the asymmetry of ions. The averaged free charge density can be calculated from the following equation and the γ-dependence for $V_0 = 1$, 5, and 10 is shown in fig. 6,

$$\overline{\rho} = \frac{1}{A}\int_A \rho \,\mathrm{d}A. \tag{13}$$

Surprisingly, we can see that $\overline{\rho}$ has almost the same value in all polygonal and circular channels irrespective of V_0, ξ and γ. In fig. 6, it is difficult to distinguish all the lines because they are almost overlapped. Because it represents the cross-sectional area average, we can conclude that we can get a similar ion enrichment irrespective of the channel shape if R_H is the same. Intuitively, however, it can be seen that as the potential increases in the lower γ regime, $\overline{\rho}$ increases steeply and can be up to several tens of times higher than the bulk concentration. On the other hand, if γ increases, the effect of the charge density increase is not large. Overall, $\overline{\rho}$ shows a monotonically decreasing tendency as γ increases. Further, when the wall potential is low ($V_0 = 1$), as expected, the change in charge density with respect to γ is insignificant. The most important consequence of this calculation is that the increase in free charge density (dashed lines) in the 1D channel is

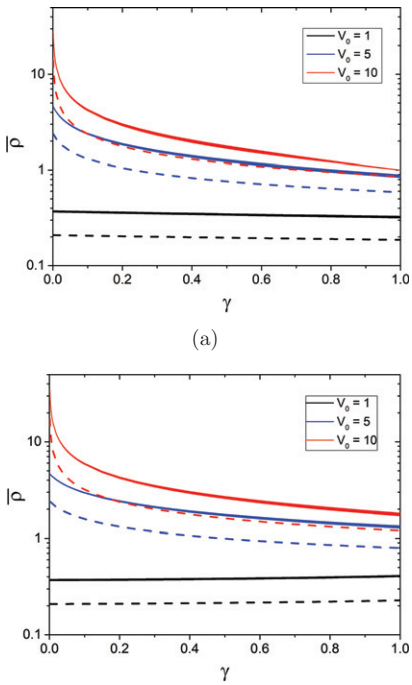

Fig. 6: (Color online) γ-dependence on $\overline{\rho}$ in 1D (dashed lines), polygonal and circular channels at (a) $\xi = 1.0$ and (b) $\xi = 0.5$ for $V_0 = 1, 5$ and 10 with $\epsilon = 0.2$.

significantly lower than that in the polygonal channels. This is because the perimeter length per area is considerably shorter than that of the polygonal channels.

Using the divergence theorem, it can be shown that the averaged free charge density over the cross-sectional area of the channel is proportional to the averaged electric field along the channel wall.

$$\int_A \rho \,\mathrm{d}A = \int_A \epsilon^2 \boldsymbol{\nabla}\cdot\mathbf{E}\,\mathrm{d}A = \epsilon^2 \oint_C E_n \,\mathrm{d}l. \tag{14}$$

Subsequently,

$$\overline{E_n} = \frac{1}{C}\oint_C E_n \,\mathrm{d}l \sim \text{const.} \tag{15}$$

That is, regardless of the shape of the polygon, the averaged E_n along the perimeter or the electric-field influx from the enclosed boundary is maintained almost constant when the same V_0 is imposed to the wall surface. In fact, a similar result can be derived from the universality of $\overline{P_{nn}}$, that is almost constant regardless of the polygon shape. From eq. (12), it can also be shown that

$$\overline{E_n^2} = \frac{1}{C}\oint_C E_n^2 \,\mathrm{d}l \sim \text{const.} \tag{16}$$

In this case, it can be seen that the average value of E_n^2, or equivalently the averaged electrical stress, is almost constant regardless of the shape of the channel, and is approximated to the average value in the circular channel. Equations (15) and (16) are very interesting results showing a

consistent trend from the low to high potential for the steric effect of ions.

Conclusion. – We explored the steric effect of electrolytes on the normal stress exerted on the wall and the free charge density in various nanoconfinements. The EDL structure near the channel wall was modified significantly by the effect of finite ion size in terms of the potential, ion concentration and osmotic pressure compared with the conventional Gouy-Chapman theory. The osmotic pressure was reduced dramatically by the ion saturation (corresponding to the tightly packed layers of ions). Consequently, the electrical stress and the normal stress exerted on the walls were modified significantly. The outward normal stress exerted on the wall and the free charge density over the cross-sections of the channels were the sensitive function of the steric factor, and the EDL structures of the equilateral polygonal channels exhibited the consistent tendency of increasing and converging from that of the 1D channel to the circular one in terms of the osmotic pressure, and the normal stress exerted on the wall. However, the averaged normal stress on the channel wall and the charge density in the channels were almost independent of the cross-section shapes of the channels. This implies that the averaged electric field flux and the averaged electrical stress are preserved irrespective of the channel shape if the hydraulic radius is the same. The universal properties of the steric effect of electrolyte in nanoconfinement will clarify our understanding on many electrohydrodynamic and electrochemical applications especially when the ion size, EDL thickness and confinement are comparable to one another in high concentration or high electric potential environments.

* * *

This research was supported by the National Research Foundation of Korea (NRF) funded by the Ministry of Science, ICT, Future Planning (NRF-2017R1D1A1B05035211) and Institute for Basic Science (IBS-R020-D1), funded by the Korean Government. This research has also been supported by the BK21 Plus program of Korea.

REFERENCES

[1] Chen J., Henderson W. A., Pan H., Perdue B. R., Cao R., Hu J. Z., Wan C., Han K. S., Mueller K. T., Zhang J. G., Shao Y. and Liu J., *Nano Lett.*, **17** (2017) 3061.

[2] Cheng X. and Pinsky P. M., *PLoS ONE*, **10** (2015) e0145422.

[3] Kornyshev A. A., *J. Phys. Chem. B*, **111** (2007) 5545.

[4] Andrews J. and Das S., *RSC Adv.*, **5** (2015) 46873.

[5] Colla T., Girotto M., Dos Santos A. P. and Levin Y., *J. Chem. Phys.*, **145** (2016) 094704.

[6] Smith W. R., Mouka F. and Nezbeda I., *Fluid Phase Equilib.*, **407** (2016) 76.

[7] Cazade P.-A., Hartkamp R. and Coasne B., *J. Phys. Chem. C*, **118** (2014) 5061.

[8] Yu J., Aguilar-Pineda G. E., Antillon A., Dong S. H. and Lozada-Cassou M., *J. Colloid Interface Sci.*, **295** (2006) 124.

[9] Das S. and Chakraborty S., *Phys. Rev. E*, **84** (2011) 012501.

[10] Kilic M. S., Bazant M. Z. and Ajdari A., *Phys. Rev. E*, **75** (2007) 021502.

[11] Kilic M. S., Bazant M. Z. and Ajdari A., *Phys. Rev. E*, **75** (2007) 021503.

[12] Colla T., Lopes L. N. and dos Santos A. P., *J. Chem. Phys.*, **147** (2017) 014104.

[13] Lee J. A. and Kang I. S., *Phys. Rev. E*, **90** (2014) 032401.

[14] Moon G. J., Ahn M. M. and Kang I. S., *Phys. Rev. E*, **92** (2015) 063020.

[15] Rajni, Oh J. M. and Kang I. S., *Phys. Rev. E*, **93** (2016) 063112.

[16] Lee J. A. and Kang I. S., *Phys. Rev. E*, **94** (2016) 043105.

[17] Bandopadhyay A., Goswami P. and Chakraborty S., *J. Chem. Phys.*, **139** (2013) 224503.

[18] Han Y., Huang S. and Yan T., *J. Phys.: Condens. Matter.*, **26** (2014) 284103.

[19] Borukhov I., Andelman D. and Orland H., *Phys. Rev. Lett.*, **79** (1997) 435.

[20] Hua C. K., Kang I. S., Kang K. H. and Stone H. A., *Phys. Rev. E*, **81** (2010) 036314.